

Deep learning framework for action prediction reveals multi-timescale locomotor control

Wei-Chen Wang¹, Antoine De Comite², Alexandra Voloshina⁴, Monica Daley^{4,5,6}, and Nidhi Seethapathi^{1,2,3,*}

¹Department of Electrical Engineering and Computer Science, School of Engineering, MIT, Cambridge, MA 02139, USA.

²McGovern Institute for Brain Research, MIT, Cambridge, MA 02139, USA.

³Brain and Cognitive Sciences, School of Science, MIT, Cambridge, MA 02139, USA.

⁴Mechanical and Aerospace Engineering, Henry Samueli School of Engineering, UC Irvine, Irvine CA 92697, USA.

⁵Ecology and Evolutionary Biology, School of Biological Sciences, UC Irvine, Irvine CA 92697, USA.

⁶Biomedical Engineering, Henry Samueli School of Engineering, UC Irvine, Irvine CA 92697, USA.

*nidhise@mit.edu

ABSTRACT

Modeling human movement in real-world tasks is a fundamental goal for motor control, biomechanics, and rehabilitation engineering. However, existing models of essential tasks like locomotion are not applicable across varying terrain, mechanical conditions, and sensory contexts. This is at least in part due to simplifying assumptions like linear and fixed timescales mappings between inputs and future actions, which may not be broadly applicable. Here, we develop a deep learning-based framework for action prediction, outperforming traditional models across multiple contexts (walking and running, treadmill and overground, varying terrains) and input modalities (multiple body states, visual gaze). We find that neural network architectures with flexible input history-dependence, like GRU and Transformer, and with architecture-dependent trial embeddings perform best overall. By quantifying the model's predictions relative to an autoregressive baseline, we identify context- and modality-dependent timescales. These analyses reveal that there is greater reliance on fast-timescale predictions in complex terrain, gaze predicts future foot placement before body states, and the full-body state predictions precede those by center-of-mass states. This deep learning framework for human action prediction provides quantifiable insights into the control of real-world locomotion and can be extended to other actions, contexts, and populations.

Introduction

Modeling human movement in real-world settings remains a major scientific challenge for motor control, biomechanics, and rehabilitation engineering. Indeed, data-driven models of essential tasks like locomotion have informed predictive simulations^{1,2}, helped characterize neuromotor disorders^{3,4}, and have been incorporated into wearable robots to anticipate the user's actions^{5,6}. Data-driven models widely used to characterize locomotor control rely on simplifying assumptions such as linear, fixed-timescale mappings or are limited to laboratory-constrained tasks. Such models have successfully explained how center-of-mass (CoM) kinematics predict foot placement⁷⁻¹⁰ and ground reaction forces^{2,11} during treadmill locomotion, but they have not been shown to generalize to real world settings. During real world movements, people exhibit more variable behaviors^{12,13}, and the control strategies may depend on the nonlinear history of multiple task-relevant inputs¹⁴. Addressing this requires a framework capable of predicting future actions given time-varying inputs from different modalities, such as body state and visual gaze, across contexts. Artificial neural networks have shown significant promise in predicting foot placement actions, as deep learning models can accurately capture the temporal and nonlinear statistics at play¹⁵. However, previous neural network models of locomotion test a single architecture¹⁶⁻¹⁸, use a single input modality^{16,17} or are confined to a single laboratory-constrained setting like treadmill walking^{18,19}. Furthermore, these data-driven models do not separate the variance explained by the input modality from the variance explained by the inter-trial variability, hindering model performance and interpretability. Here, we put forth a deep learning framework comparing multiple neural network architectures, with architecture-dependent trial embeddings, outperforming existing models across real world contexts.

Biological motor control is time-varying and context-dependent, requiring adaptive strategies to meet environmental, task-specific, and physiological demands²⁰. For example, during locomotion, humans possess a remarkable ability to continuously modulate their actions in diverse "contexts" i.e. environment-specific circumstances such as uneven terrain or obstacle-avoidance^{21,22}. This ability is supported by dynamic sensorimotor control strategies that can be deployed both on a fast timescale such as during each walking step, or on a longer timescale over multiple steps^{22,23}. For instance, walking on uneven

terrain requires rapid adjustments to foot placement²⁴, as well as persistent motor plans involving path or speed selection²⁵. In fact, multiple timescales in motor control have been hypothesized to reflect distinct neural computations²⁶ or distinct functional goals²⁷, so quantifying multi-timescale control strategies from real world data has theoretical value. Despite this, we lack meaningful approaches to quantify multi-timescale control in real world contexts. Here, we put forth the predictive power of nonlinear action prediction models relative to an autoregressive baseline as a generalizable way to quantify control timescales, discovering a context-dependent tradeoff between fast- and slow-timescale predictions.

Biological sensorimotor control is achieved by dynamically mapping multi-sensory inputs to motor commands, enabling adaptive control in changing contexts^{28,29}. During locomotion, the control of foot placement is inherently multimodal, and prior work has examined the role of individual input modalities such as vision²⁴ or low-dimensional body states on control⁷. Visual input is crucial for anticipatory locomotor control when navigating obstacles or selecting stable footholds on complex terrains^{13,30}, while joint-level or CoM-based feedback informs muscle responses to transient perturbations^{2,31,32}. Vestibular input is also thought to guide foot placement, particularly in a phase-dependent manner³³. Despite the existence of multiple input modalities, existing foot placement control models assume a linear fixed control timescale with low-dimensional body states as an input^{7,34}, thereby neglecting the temporal dynamics of how and when each modality contributes to control, and how different modalities compare to one another. To address these gaps, we propose a data-driven framework that systematically evaluates the contributions of multiple input modalities — including CoM-relevant kinematics, full-body kinematics, and gaze fixations — to predicting future foot placement. By comparing the predictive power of each modality to an autoregressive baseline model, we quantify the timescale and magnitude of modality-dependent foot placement. Our framework reveals at which phase of the gait cycle each input modality become critical for informing future foot placement.

In this study, we develop deep learning-based models to predict future actions from multimodal input time series and test them in diverse locomotor tasks. By comparing different model architectures, we find that architectures with flexible input history-dependence generalize better across real-world contexts and input modalities. We characterize the control timescale of a given nonlinear action prediction model using its predictive power relative to an autoregressive baseline model, to help reveal how these timescales are shaped by the context and the input modality. Our work has implications for characterizing, modeling, and predicting real world movements and the multi-timescale control strategies hidden in them. This deep learning framework can inform the development of human-aware wearable robot control and more human-like physics-based simulations of motor behavior in the real world^{35,36}.

Results

In this section, we present findings using our deep learning framework for action prediction to understand the influence of the environmental context and input modality on future foot placement. First, we demonstrate that neural network models, particularly GRUs, significantly outperform linear models in more challenging contexts. During overground walking, we find that subjects exhibit a tradeoff between fast and slow timescale predictions, with the magnitude of the tradeoff varying across different terrains. By comparing the predictive power of input modalities to an autoregressive baseline model, we reveal that control timescales are both modality- and context-dependent. Finally, we discover a gait phase mid-swing when the swing foot dynamics becomes useful for foot placement prediction. We encourage readers to first read through the *Methods* section to understand the terminology used below. An overview of the key methodological components in the deep learning framework can be found in Figure 1.

Models with flexible nonlinear input dependence outperform linear models

We evaluated the performance of nine models — LSTM, GRU, FCNN, TCN, Transformer, Linear instance with (LI2) and without (LI) L2 regularization, Linear history with (LH2) and without (LH) L2 regularization — on their ability to predict foot placement across various tasks and input modalities. The tasks included treadmill walking, treadmill running, and overground walking on various terrains, while the input modalities consisted of CoM-relevant kinematics, full-body kinematics, swing-foot kinematics and gaze fixations. The model score was evaluated based on the Root Mean Squared Error (RMSE) relative to the optimal model at each gait phase, and then normalized by the highest-scoring model. The Methods section details the evaluation metric.

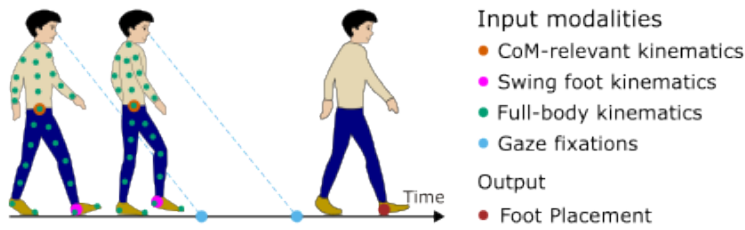
Our analysis reveals that during treadmill walking and running, the locomotor control strategies can be effectively captured by linear models, particularly model LI2. Among the tested architectures, GRU demonstrates the best overall performance, followed closely by Transformers and LSTM (Table 1). Since GRU demonstrates the best overall performance, it is used for the analyses in the subsequent sections. An exception arises when using gaze fixations as the input modality during flat terrain overground walking, where Transformers significantly outperform all other models. However, this is also the only modality and context where predictive power never surpasses the baseline model, suggesting that gaze does not play a significant role in foot placement prediction. To examine the temporal trends of each model more closely, we provide the RMSE as a function of gait phases for each model under different conditions in Figures 6 and 7. We find that FCNN performs better during treadmill

Deep learning framework for action prediction across tasks and contexts

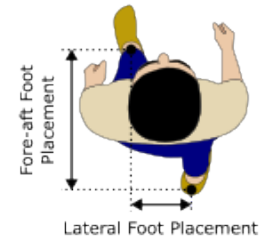
A Diverse tasks and contexts



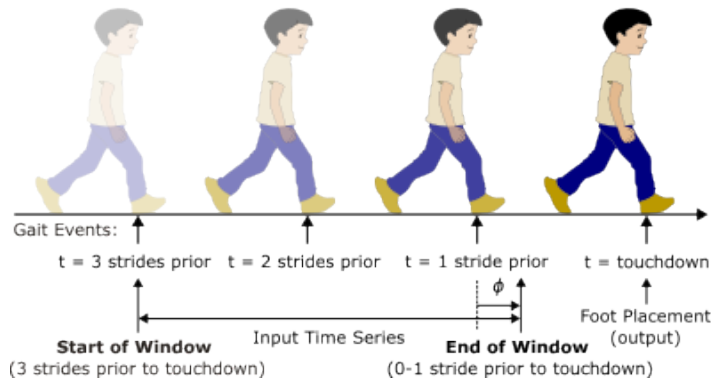
B Inputs and outputs



C Foot Placement



D Input timing and window



E Network architecture

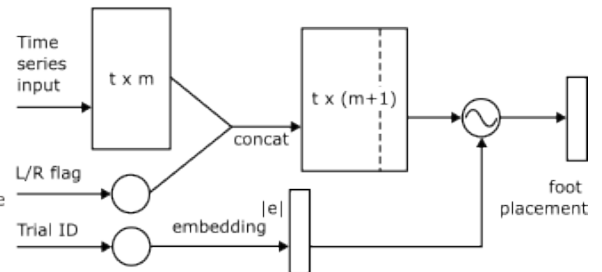


Figure 1. Overview of the deep learning framework. **A** We include diverse tasks and contexts, including overground walking with various terrain conditions, treadmill walking, and treadmill running on even and uneven terrain. **B** Inputs contain hypothesized modalities such as CoM-relevant kinematics, swing-foot kinematics, full-body kinematics, and gaze fixations (defined by the intersection of the gaze vector with the ground plane). The output is foot placement. **C** Foot placement output is defined by the lateral and fore-aft foot placement relative to the opposite foot at its previous heel strike. **D** The input is a time series spanning from three strides prior to touchdown to a specific gait phase within the previous stride. The output corresponds to foot placement at heel strike. We denote the ending gait phase of the time series relative to one stride prior to touchdown as ϕ , discretized and sampled from $n = 21$ equally spaced phases within $0 \leq \phi \leq 1$. **E** The network architecture of the nonlinear models. The input consists of a time series, an L/R flag, and a trial ID. The time series and L/R flag are concatenated, while the trial ID is embedded to provide additional trial-specific information. The incorporation of this embedding is architecture-dependent, i.e. it influences the model prediction differently depending on the neural network architecture, as detailed in the Methods section.

| Task | Terrain | M | LSTM | GRU | FCNN | TCN | Trans | LI | LH | LI2 | LH2 |
|------|---------|---|------|------|------|------|-------|------|------|------|------|
| TW | N/A | C | 1.00 | 1.00 | 0.98 | 0.71 | 0.98 | 0.97 | 0.26 | 0.97 | 0.99 |
| TR | Even | C | 0.98 | 1.00 | 0.96 | 0.92 | 0.98 | 1.00 | 0.34 | 1.00 | 0.97 |
| | | F | 1.00 | 1.00 | 0.89 | 0.82 | 0.94 | 0.38 | 0.62 | 1.00 | 0.78 |
| | Uneven | C | 0.98 | 1.00 | 0.96 | 0.91 | 0.97 | 0.97 | 0.31 | 0.97 | 0.97 |
| | | F | 1.00 | 1.00 | 0.93 | 0.91 | 0.96 | 0.35 | 0.63 | 0.99 | 0.76 |
| OW | Flat | C | 0.96 | 1.00 | 0.95 | 0.94 | 0.99 | 0.91 | 0.70 | 0.95 | 0.88 |
| | | F | 0.97 | 0.99 | 0.94 | 0.95 | 1.00 | 0.52 | 0.76 | 0.87 | 0.77 |
| | | V | 0.80 | 0.87 | 0.70 | 0.91 | 1.00 | 0.69 | 0.30 | 0.75 | 0.30 |
| | Medium | C | 0.96 | 0.99 | 0.95 | 0.98 | 1.00 | 0.86 | 0.66 | 0.93 | 0.78 |
| | | F | 0.97 | 0.98 | 0.94 | 0.99 | 1.00 | 0.52 | 0.76 | 0.82 | 0.77 |
| | | V | 0.95 | 0.98 | 0.88 | 1.00 | 0.97 | 0.68 | 0.32 | 0.75 | 0.33 |
| | Rough | C | 0.99 | 1.00 | 0.97 | 0.99 | 1.00 | 0.31 | 0.68 | 0.87 | 0.73 |
| | | F | 0.99 | 0.99 | 0.94 | 0.98 | 1.00 | 0.58 | 0.74 | 0.74 | 0.74 |
| | | V | 1.00 | 1.00 | 0.92 | 0.96 | 0.97 | 0.34 | 0.61 | 0.61 | 0.61 |

Table 1. Normalized Model Scores across Tasks and Input Modalities. Models were evaluated on treadmill walking (TW), treadmill running (TR), and overground walking (OW) tasks with varying terrain. The input modalities (M) were: CoM-relevant kinematics (C), full-body kinematics (F), and visual gaze (V). The normalized model scores use the following color coding: dark green (0.98–1.00), light green (0.95–0.98), orange (0.90–0.95), and red (< 0.9). Normalized model scores, defined in the Methods section, are rounded to two decimal places, potentially resulting in two models having a score of 1.00 (e.g., the other model’s score could be 0.997).

locomotion, but poorly during overground walking, whereas TCN performs poorly during treadmill locomotion, even worse than some linear models, but better during overground walking. While linear models are sufficient to capture the relationship between input modality and foot placement during treadmill movements, nonlinear models are necessary to account for the history-dependence and inherent nonlinearities of the input modality in non-stationary contexts (Table 1).

Fast- versus slow-timescale predictions are context-dependent

Biological motor control exhibits remarkable adaptability, seamlessly combining fast- and slow-timescale control strategies, depending on task complexity and other environmental demands. Here, we quantify multi-timescale tradeoffs as a function of varying terrains. We define the tradeoff between fast- and slow-timescale predictions as the relationship between CoM-relevant prediction intercept and its peak predictive power relative to the autoregressive baseline. The intercept is defined by the R^2 value at gait phase 0 (Figure 2A), quantifying the degree of long-timescale prediction. We obtain the relative predictive power (ΔR^2) by subtracting the baseline predictive power from the R^2 , and define the peak relative predictive power as maximum ΔR^2 . While trials exhibit varying intercepts, the intercepts of CoM-relevant kinematics and the baseline are highly correlated (Figure 2B; $r = 0.97$). By subtracting baseline predictive power from predictive power, this relative measure reduces inter-trial variability, enabling a more meaningful comparison across trials.

During overground walking on flat terrain, the negative correlation reveals a tradeoff between long- and short- timescale prediction, indicating that trials that rely more heavily on long-timescale prediction shows a reduced dependency on short-timescale prediction (Figure 2C, $r = -0.69$). As terrain becomes rougher, subjects exhibit less long-timescale prediction, leading to a decrease in the intercept of CoM-relevant kinematics, thereby reducing the magnitude of the correlation with the peak relative predictive power (Figure 2C; $r = -0.5$ on medium terrain, $R = 0.02$ on rough terrain). Further analysis of the slope between the peak of the relative predictive power and the intercept reveals additional insights; the negative sign of the slope confirms a tradeoff between long- and short-timescale predictions, while the slope magnitude represents the rate at which long-timescale prediction decreases as short-timescale prediction increases. We observe that the tradeoff magnitude changes across terrain variations, reflecting a change in long- and short-timescale prediction of foot placement (Figure 2D).

Relative predictive power reveals different control timescales across modalities

Human locomotion involves dynamic integration of multiple sensory inputs to guide future foot placement. Our framework seeks to uncover how humans utilize various input modalities, including CoM-relevant kinematics, full-body kinematics, and gaze fixations, across varying contexts like treadmill walking⁷, treadmill running³⁷, and overground walking on terrains of different roughness³⁰. To understand the predictive ability of the input modality, we train a model that takes the time series of the input modality and predicts the future foot placement. As the input time window increases, the model demonstrates improved predictive power, as shown by a closer alignment between predictions and ground truth (Figure 3A). The results demonstrate how different input modalities influence foot placement prediction across contexts. By analyzing the relative predictive power (ΔR^2) of modality-based models compared to the autoregressive baseline, we obtain the timing and magnitude of each modality's contribution to foot placement control (Figure 3B).

During overground walking on flat terrain, gaze does not play a significant role in foot placement prediction, as its performance does not surpass the autoregressive baseline (Figure 3C). This suggests that foot placement control on flat terrain is not guided by gaze. Across contexts, full-body kinematics begin to outperform the baseline earlier than CoM-relevant kinematics; we provide some possible explanations in the discussion section. Despite the inclusion of significantly more body markers (29 vs. 1), full-body kinematics only explained 6-14% of additional foot placement variance, which highlights the significance of CoM-relevant kinematics in locomotor control (Figure 3C). As terrain complexity increases, foot placements are better predicted by gaze, with predictions earlier than both CoM-relevant and full-body kinematics for lateral (Figure 3C) but not fore-aft (Figure 8C) adjustments. This indicates that in more challenging environments, humans rely on visual gaze to inform lateral foot placement in advance of the body states. Across contexts and modalities, lateral foot placement control occurs earlier than fore-aft control, indicating a prioritization of lateral stability during locomotion (Figure 8A), which aligns with previous findings^{7,38,39}. During treadmill running, the relative predictive power for lateral foot placement is not significantly different between even and uneven terrain. However, the fore-aft foot placement predictions is earlier during on uneven than on even terrain (Figure 8B). This discrepancy is likely a result of solely fore-aft terrain perturbations introduced in the uneven terrain running study³⁷.

The swing foot dynamics predict future foot placement mid-swing

Swing foot dynamics are essential for understanding how humans adapt their locomotion strategies to varying terrains and tasks. In prior work, it is implicitly assumed that swing foot prediction occurs simultaneously with the timing of swing initiation^{11,40}. To analyze these dynamics, we detect the timing of swing initiation by identifying when the swing foot's velocity in the direction of locomotion exceeds 5% of its peak velocity (Figure 5B). During overground walking, swing initiation occurs significantly later than during treadmill walking (Wilcoxon signed-rank test, one-sided, $p < 0.05$; Figure 4A). As the terrain

Relative predictive power reveals fast and slow timescales across contexts

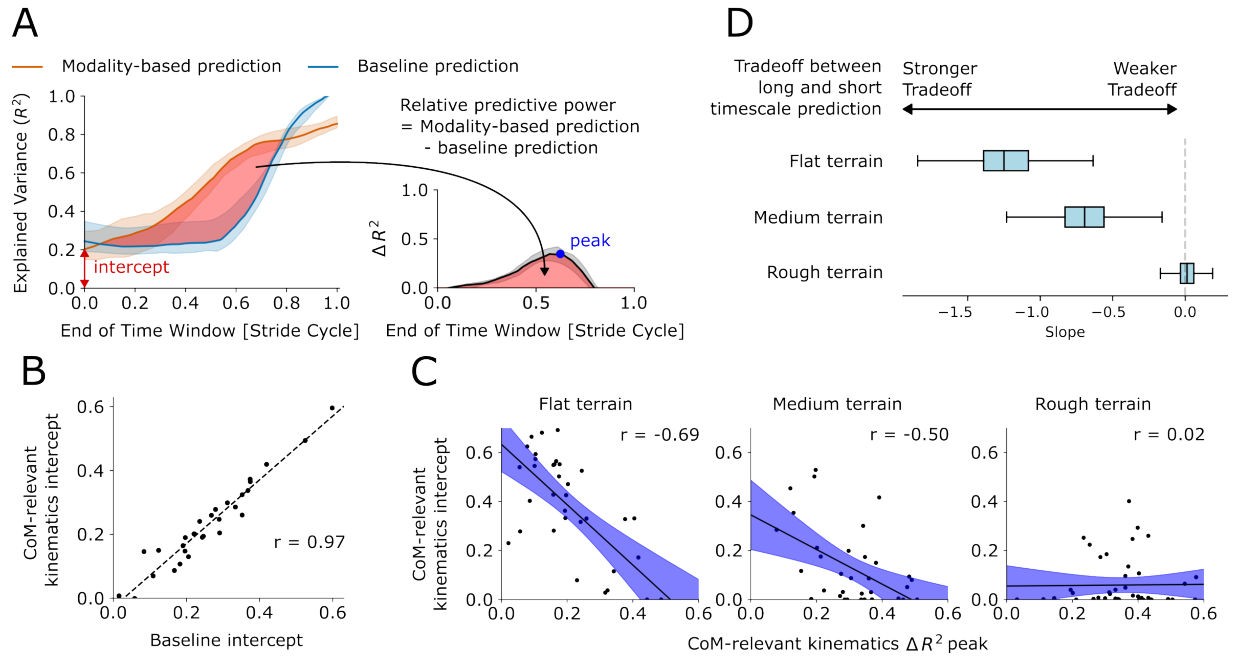


Figure 2. Relative predictive power reveals fast and slow timescales across contexts. **A** Explained variance (R^2) as a function of gait phase for modality-based (orange) and autoregressive baseline (blue) predictions. The intercept is defined as the modality-based R^2 value at gait phase 0 (i.e., the input time series spans from three gait cycles prior to touchdown and ends one gait cycle before touchdown). The red shaded area represents the relative predictive power (ΔR^2), calculated as the difference between modality-based and baseline predictions. The peak is the maximum ΔR^2 . **B** Baseline intercept versus CoM-relevant kinematics intercepts for treadmill walking. **C** Relationship between the CoM-relevant kinematics intercepts and peak ΔR^2 during overground walking across terrains with linear regression fits. The plots display the regression line and 95% confidence interval. **D** Coefficients between CoM-relevant kinematics ΔR^2 peak and intercept of CoM-relevant kinematics. The box-plot shows the median (bar in box), 25 – 75% percentile (box), and non-outlier range (whiskers) of the bootstrap statistics. The magnitude of the slope quantifies the strength of the tradeoff between long- and short-timescale prediction.

Relative predictive power reveals modality-dependent control timescales

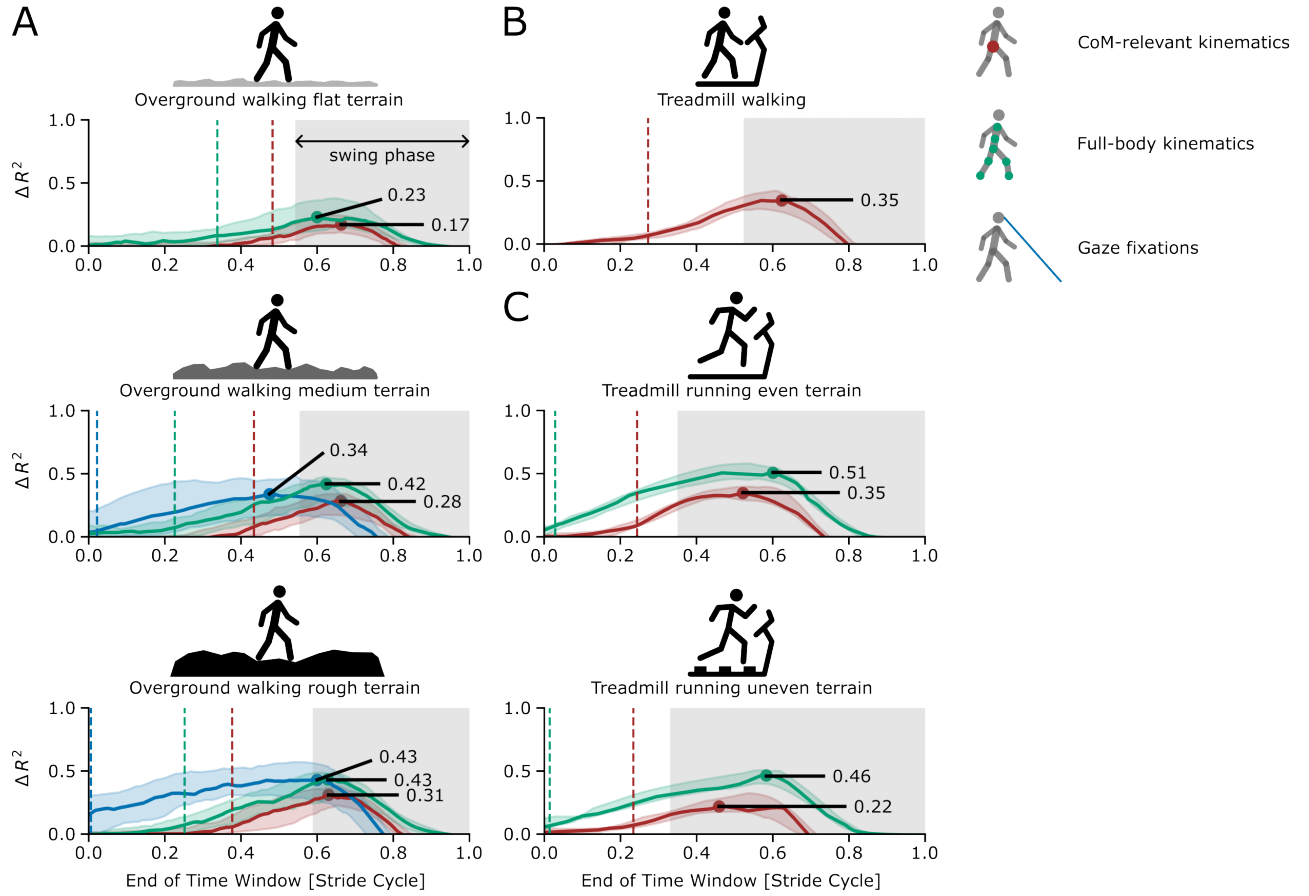


Figure 3. Relative predictive power reveals modality-dependent control timescales. **A** Relative predictive power (ΔR^2 , median and interquartile range) of CoM-relevant kinematics, full-body kinematics, and gaze fixations for overground walking on different terrain roughness. The highlighted interval begins when ΔR^2 exceeds 5% (Wilcoxon, one-sided), and ends at the peak ΔR^2 . The shaded area represents the swing phase. **B** Relative predictive power of CoM-relevant kinematics for treadmill walking. **C** Relative predictive power of CoM-relevant kinematics and full-body kinematics for treadmill running on even and uneven terrains.

becomes rougher, the timing of swing initiation is further delayed, perhaps reflecting the need to gather additional information for precise foot placement on a stable foothold. In contrast, running exhibits different swing foot prediction dynamics⁴¹, characterized by the absence of a double stance phase and the presence of a flight phase, where neither foot is in contact with the ground. These features allow for much earlier swing initiation. Similarly, during treadmill running on uneven terrain, swing initiation occurs later, consistent with the increased demands of navigating complex environments.

The timing at which the swing foot begins to contain significant information regarding foot placement (“breakpoint” timing, Figure 5C) provides further insight into the swing foot prediction dynamics. During treadmill walking, lateral foot placement prediction (FP) timing occurs significantly later than the swing foot initiation (Wilcoxon signed-rank test, one-sided, $p < 0.05$; Figure 4B), indicating that the swing foot does not contribute substantial information to foot placement immediately after the swing begins. However, no significant difference is observed between swing timing and fore-aft FP timing. This finding is consistent with overground walking on flat terrain, where lateral FP timing occurs later than swing timing, while fore-aft FP timing does not exhibit such a delay (Figure 4C). As terrain complexity increases during overground walking, both lateral and fore-aft FP timing are delayed relative to swing timing, perhaps reflecting the additional planning demands imposed by rougher terrains. A similar delay is observed during treadmill running, where both lateral and fore-aft FP timing occur much later than swing initiation. This is likely due to the earlier swing initiation in running driven by the flight phase, while the swing foot does not contribute significant information about foot placement until later in the gait cycle (Figure 4C). These findings highlight how swing foot prediction dynamics are adapted to environmental and task-specific demands, and that swing initiation does not necessarily coincide with the point at which the swing foot begins to contain significant information about foot placement.

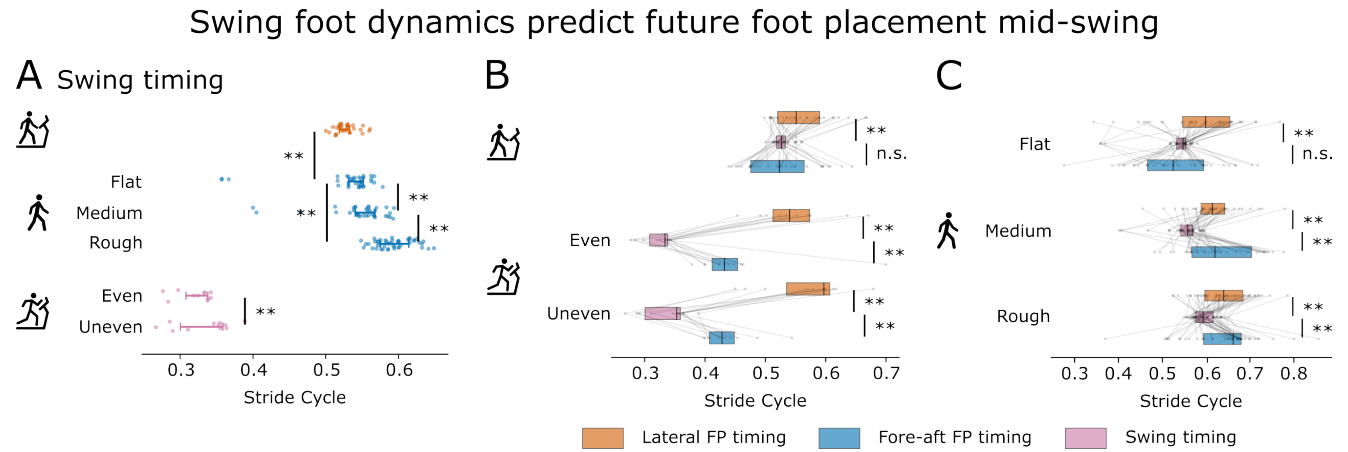


Figure 4. Swing foot dynamics predict future foot placement mid-swing. **A** Timing of when the swing foot starts to swing across different contexts. **B, C** Comparison of the timing when the swing foot starts to swing with the timing of when the swing foot begins to provide significant information about foot placement, detected using the average slope method (Figure 5C), during treadmill (**B**) and overground (**C**) movements. ** for $p < 0.01$; n.s. for not significant.

Discussion

In this study, we present a data-driven framework to characterize real-world motor behaviors by how much and when different input modalities predict future actions. We incorporate trial embedding information into the framework in an architecture-dependent manner, which enables the models to separate trial-specific explained variance from the variance explained by the input modality. By employing deep learning models that incorporate the temporal history of state estimates, we outperform simpler models in non-stationary tasks for predicting future foot placements. We compare the predictive power of various hypothesized input modalities (e.g., center-of-mass kinematics, full-body kinematics, and gaze fixations) against an autoregressive baseline. This baseline comparison reduced the impact of inter-trial variability, allowing us to isolate and interpret the context- and modality-dependent effects more clearly. We quantify the contribution of each modality to foot placement through their distinct prediction timescales. We discover a tradeoff between long- and short-timescale predictions across contexts; in more uncertain contexts like rough terrain, we find a reduced reliance on long timescale predictions. Finally, rather than assuming that foot placement is initiated at the very start of the swing cycle, our method helps identify the swing phase at which the foot begins to carry significant predictive information about the foot placement location. Together, these findings highlight multi-timescale control strategies in real world locomotion, revealing how they are shaped by the task context and the input modality. Our framework can be extended to analyze other input modalities and motor actions to characterize real world motor behavior.

Comparing different model architectures in their ability to predict foot placement. The model performances across tasks and input modalities (Figure 1) highlight the strengths and limitations of various network architectures. During laboratory-constrained treadmill locomotion, linear models demonstrate performance comparable to the best-performing nonlinear models. This suggests that control strategies during treadmill locomotion is relatively simple and linear^{42,43}, and therefore can be effectively captured by existing models that assume fixed-timescale linear mappings^{2,7}. Interestingly, the Temporal Convolutional Network (TCN) performed worse than linear models, which can be attributed to its rigid structural design, especially its reliance on fixed-size convolutional kernels and local receptive fields. On treadmill locomotion tasks, where there is less input history-dependence, fully connected neural network (FCNN) performs well as a result of the simplicity and linearity of the mappings⁴⁴. During overground walking, we observe that GRUs⁴⁵ and Transformers⁴⁶ perform the best, since their gating or attention mechanisms enables the models to dynamically focus on the most relevant timesteps. This implies that the task demands are more non-stationary, and there may be varying temporal dependence on input history. While existing models, which are predominantly simple and linear, provide valuable insights into foot placement control in constrained environments like treadmill walking^{2,7,11}, they fail to capture the complexity of more naturalistic locomotion such as overground walking. During overground walking, TCNs show comparable performance to other nonlinear models, as their ability to process long-term dependencies becomes more relevant^{47,48}. In contrast, the FCNN now performs the worst among nonlinear models, highlighting the benefits of architectures that specialize in time series prediction in non-stationary scenarios. This is consistent with prior work showing that models explicitly designed for sequential data often outperform generic architectures in handling temporal dependencies⁴⁹⁻⁵¹.

Tradeoffs between long- and short-timescale action predictions. Our study identifies long- and short-timescale control strategies hidden in real-world movement data (Figure 2A). Previous research has highlighted the importance of fast-timescale within-step corrections, such as those used for obstacle avoidance or unexpected terrain changes to enable stable locomotion^{7,52,53}, showing that these corrections have a stabilizing effect on the body. Studies that have analyzed gaze fixations, on the other hand, have identified longer-timescale control strategies³⁰, but have not tested whether these co-exist with or replace fast-timescale strategies. This gap is important to address, because the hierarchical motor control hypothesis posits the existence of both low-level fast timescale and high-level slow timescale processes^{27,54}. Here, we discover the existence of both gaze-predictive long timescale and body state-predictive fast timescale control strategies during natural locomotion. For walking on uneven terrain with varying complexity, we discover a context-dependent tradeoff between slow- and fast-timescale prediction (Figure 2C). We interpret this tradeoff to reflect the greater prioritization of fast-timescale strategies in more complex environments, due to the rapid changes in the environmental statistics as a function of time. This tradeoff could be explained as the outcome of an optimization process in which working-memory resources used to represent the environment are allocated efficiently²¹, relying on more recent information in more complex environments. Indeed, while optimal feedback control suggests that there is more reliance on feedback in the presence of uncertainty⁵⁵⁻⁵⁷, here we provide evidence to support this normative hypothesis in a real world settings (Figure 2C). Our model advances the understanding of how predictive planning and reactive corrections are balanced in dynamic environments, highlighting the efficiency of the motor control system in integrating long- and short-timescale strategies to achieve smooth and adaptive movements.

Input modality-dependent timescales for motor control. By analyzing the relative predictive power of different input modalities our approach enables identification of when each modality becomes useful for planning future actions (Figure 3). Specifically, we find that full-body kinematics predict future foot placement earlier than CoM-relevant kinematics during treadmill running and overground walking. This earlier full-body prediction could be explained by the hypothesis that preparatory actions distributed across body segments may provide early cues to help modulate the CoM's state⁵⁸. Alternatively, earlier full-body predictions could be explained by the correlation with features not captured by the CoM state such as whole-body angular momentum and its role in foot placement prediction^{59,60}. We also found that the utilization of CoM-relevant kinematics is delayed during overground walking compared to treadmill walking. This delay likely stems from the increased variability in terrain and the demands of path planning in overground environments, which require more time to integrate information needed to determine optimal foot placement^{61,62}. Additionally, as terrain roughness increases, there is a greater reliance on gaze, as evidenced by the increasing relative predictive power of gaze fixations as an input modality^{13,22}. Previous work has demonstrated that humans use visual information for path planning on complex terrain, actively avoiding steep steps with large height changes in favor of flatter, more circuitous paths²⁵. Our findings further suggest that visual inputs are primarily utilized for lateral foot placement (Figure 3E) rather than fore-aft placement (Figure 8) on uneven terrains, which aligns with previous findings that humans tend to adjust step width rather than step length to avoid obstacles^{63,64}. Future studies could build on our data-driven approach to provide insight into the control mechanisms underlying these modality-dependent timescales.

Conclusions and future work. Our work highlights how complex real world movement data can be combined with data-driven approaches to obtain insight into the control strategies at play. We put forth a deep learning framework for action prediction, finding that nonlinear models outperform traditional linear models by capturing the input history-dependence at

play in real world contexts. Our framework provides a comprehensive and generalizable approach to compare the influence of different input modalities and contexts on the control strategies chosen. By identifying specific phases when there is more predictive ability, it provides new insight into the temporal structure of motor planning and control in high-dimensional tasks. Overall, we present a behavioral data-driven approach that future work can build on to understand context- and modality-dependent control strategies in everyday movements. Our approach can be extended to analyze large-scale data across different motor behaviors^{65,66} and species^{67,68}. Integrating the context- and modality-dependent timescales identified by our approach into physics-based models could yield more human-like simulation and clarify the underlying neuromechanics^{69–71}. These data-driven models can also enable more human-like assistive robots that generalize better across environmental contexts or more directly incorporate gaze data to inform control.

Methods

In this section, we present the data-driven framework for analyzing and inferring control strategies across contexts. First, we describe the datasets used in this study and how the inputs and outputs for the models were structured. Next, we introduce the linear and nonlinear models used to map the hypothesized input modalities to foot placement. We further provide details on the training and evaluation procedures for these models, and discuss the statistical tests employed to examine the prediction timescale.

Data Description and Processing

Our framework is versatile and can be applied to any dataset with time-series inputs and discrete output events. To demonstrate this flexibility, we utilized several existing datasets of human locomotion across a range of contexts (Figure 1A), including walking and running on both treadmills and overground, as well as across uneven terrain. The treadmill walking dataset was collected by Wang and Srinivasan⁷, while the treadmill running dataset on even and uneven terrains was collected by Voloshina and colleagues³⁷. The overground walking dataset, collected by Matthis and colleagues³⁰, includes full body kinematics of subjects walking on flat, medium, and rough terrains alongside gaze information recorded to track ground fixations during locomotion.

For all studies, we processed kinematic data by a zero-lag 4th order Butterworth lowpass filter (cutoff frequency of 6 Hz). Here, let x denote the lateral direction, y denote the fore-aft direction, and z denote the vertical direction. For treadmill movement datasets, the fore-aft marker positions were adjusted to account for belt speed to allow direct comparisons with overground data. Formally, let $y(t)$ denote the forward position of any marker at time t , the adjusted fore-aft position is defined as $y'(t) = y(t) + v \cdot t$, where v is the belt speed. For overground data, the fore-aft axis was aligned with the main direction of locomotion, such that the pelvis position starts at $(0,0)$ on the x - y plane and moves towards the positive y -axis. We computed the velocity of each marker using 4th order centered finite differences of their positions. Next, we computed the heel strike timings as the time at which the fore-aft distance between the foot and the pelvis markers is maximal⁷². While other gait segmentation procedures based on velocity threshold produce similar estimates of contact detection⁷³, we chose to adopt the method based on the relative foot position as it was more robust to noise during overground locomotion. We segmented the data into individual gait cycles and temporally interpolated them into 20 equally spaced gait phases. We implemented several tests to detect and discard abnormal gait cycles. These tests verified whether the stance foot was fixated on the floor during the stance phase (walking data only), and whether the timing of each heel strike was coherent with neighboring heel strikes. Overall, less than 0.1% of the steps were discarded for treadmill walking and running, while less than 2% of the steps were discarded for the overground locomotion dataset.

Modeling Framework

Foot placement control depends on the history of input modalities, such as postural or gaze information. In this study, we leveraged deep learning techniques to evaluate the correlations between various input modalities and future foot placement (see Figure 1 for an overview of the modeling framework).

We hypothesized that different input modalities are integrated throughout locomotion to inform future foot placements. These modalities include the CoM-relevant kinematics, the swing-foot kinematics, the full-body kinematics, and the gaze fixations (Figure 1B). The output predicted by the models consists of the lateral and fore-aft foot placement relative to the contact location of the opposite foot at heel strike (Figure 1C). In this study, we leveraged deep learning models to evaluate the relationships between these input modalities and the future foot placement. Let $v_i \in \{0, 1, \dots, T-1\}$ be the trial ID of data point i , where T is the number of trials, and $l_i \in \{0, 1\}$ be the left-right (L/R) flag of data point i , representing whether the corresponding output data point is a left (0) or a right (1) heel strike. The time series capturing the input modalities is denoted by $\mathbf{S}_i = [\mathbf{s}_i^{(1)}, \mathbf{s}_i^{(2)}, \dots, \mathbf{s}_i^{(m)}]$, where m is the number of features, and $\mathbf{s}_i^{(j)}$ is the j -th feature of the time series. This time series starts 6 steps prior to the predicted heel strike (Figure 1D) and its end is sampled from the previous gait cycle with 20 equally spaced gait phases. This range is chosen because 6 steps is a reasonable upper bound of how much subjects plan their foot

placement ahead, while 2 steps is a reasonable lower bound^{2,7,30}. Let ϕ denote the gait phase relative to one gait cycle prior to heel strike (i.e. previous heel strike of the same foot). With the dataset sampled at 20 time steps per gait cycle, the length of $\mathbf{s}_i^{(j)}$ ranges from 41 (when time series ends at $\phi = 0$) to 61 (when time series ends at $\phi = 1$). We define the concatenated inputs as $X = \{x_i\}_{i=1}^n$, where $x_i = \{\mathbf{S}_i, v_i, l_i\}$, and seek to obtain the mapping between those inputs X and the outputs $Y = \{y_i\}_{i=1}^n$, where $y_i = [f_i^{ML}, f_i^{AP}]$ where f_i^{ML} and f_i^{AP} represent the mediolateral (ML) and anteroposterior (AP) foot placement, respectively.

Nonlinear models

Training deep learning models typically requires large amounts of data⁷⁴, which is challenging with locomotion as most datasets only capture a few minutes of data for each trial. Therefore, it is often impractical to train deep learning models tailored to specific subjects or trials. To address this limitation, we pooled the data from all trials and train a unified model that includes trial ID as an input. By doing so, the model can learn trial-specific variations in a data-driven way while efficiently leveraging the entire dataset (Figure 1E). We first reshaped the left-right flag l_i to match the time series input's dimension and concatenated them, which resulted in a matrix of shape $(t, m + 1)$, where m is the number of features in the time series. The trial ID was embedded⁷⁵ into a vector E of length $|E| = \lceil \sqrt{T} \rceil$ and integrated with the time series data in a manner that is dependent on how each neural network processes the timesteps. The embedding enables us to isolate the inter-trial variability from the context- and modality-specific variability, which are the focuses of this study. The models we used include:

1. Long Short-Term Memory Model (LSTM)⁷⁶: The trial embedding is passed through a fully connected layer to transform it into a vector matching the size of the LSTM hidden layer. This transformed embedding is used to initialize the hidden state of the LSTM⁷⁷. The LSTM then processes the time series sequentially with gating mechanisms, leveraging this trial-specific initialization. Finally, the output of the LSTM is passed through a fully connected layer with a rectified linear unit (ReLU) to predict the foot placement.
2. Gated Recurrent Units (GRU) Model⁴⁵: Similar to LSTM with the exception that the LSTM architecture is replaced by a GRU one. Specifically, GRU has fewer parameters compared to an LSTM model.
3. Temporal Convolutional Network (TCN)⁴⁷: Unlike the LSTM and GRU models, the TCN processes the time series using convolutional layers to capture temporal dependencies in parallel instead of sequentially. The trial embedding is concatenated with the time series along the feature axis before being passed into the TCN. The TCN architecture consists of two dilated convolutional layers with downsampling and residual connections to effectively model temporal dependencies. The output of the TCN block is then passed through fully connected layers with ReLU activation to predict foot placement.
4. Transformer⁴⁶: The Transformer model leverages self-attention mechanisms to capture temporal dependencies in the time series. The trial embedding is concatenated with the time series along the time axis, allowing the model to incorporate trial-specific information. The architecture includes a feature embedding layer, positional encoding to preserve temporal order, and a Transformer encoder consisting of multi-head self-attention and feedforward layers. The output of the encoder is aggregated and passed through two fully connected layers with ReLU activation to predict the foot placement.
5. Fully connected neural network (FCNN): We explored architectures not specifically designed for time series data. In this approach, the time series is first flattened into a single vector, resulting in a feature vector of shape $tk + |E| + 1$, where t is the number of timesteps, k is the number of features, and $|E|$ is the dimension of the trial embedding. This vector is then passed through a fully connected neural network with multiple layers and ReLU activations. The network architecture employs a progressive reduction in the number of nodes per layer, controlled by a decay parameter, which determines both the total number of layers and the rate at which the node count decreases in each subsequent layer.

Linear models

For linear models, we train one model for each trial for two key reasons. First, linear models are less data-intensive and can effectively be trained on the limited data available within individual trials. Second, linear models lack the representational capacity to leverage trial-specific embeddings. By training trial-specific models, we ensure that the unique relationships within each trial are accurately captured and that the models are evaluated fairly.

1. Linear instance (LI): Instead of analyzing the entire time series, we focus on a linear model that utilizes only the last instance of the time series (i.e. the body state at a particular gait phase). We fit a linear regression model to the last row vector of the time series input. This approach is similar to the models presented in⁷.
2. Linear history (LH): The time series input is flattened into a vector of shape tk , and an Ordinary Least Squares regression is fitted to the data.

3. Linear instance with L2 regularization (LI2): L2 regularization (Ridge regression) is applied to the linear instance model to reduce overfitting.
4. Linear history with L2 regularization (LH2): L2 regularization (Ridge regression) is applied to the linear history model to reduce overfitting.

Model Evaluation and Baseline Model

Nested cross-validation was employed to evaluate the models' performance and hyperparameter tuning, ensuring an unbiased estimate of model performance and preventing data leakage⁷⁸. The dataset was initially split into five equal folds. In each iteration of the outer loop, 80% of the data was allocated for training and validation, while the remaining 20% was held out as the testing set. The training/validation set was further subdivided into five inner folds. Four inner folds were used to train the model, and the remaining fold was used for early stopping, with a patience of 50 epochs. This process was repeated for every combination of hyperparameters, with parameter updates performed using the ADAM optimizer⁷⁹ and a learning rate of 0.001. We used mean squared error (MSE) as the loss function. After each training session, the model's performance was evaluated on the outer testing fold. The outer loop was repeated five times, ensuring that each data point in the original dataset was used once for testing and four times for training/validation.

Optimal hyperparameters for each modality and dataset were first identified using grid search (or random search for large hyperparameter spaces exceeding 100 configurations; see Appendix for details). These hyperparameters were then used in the nested cross-validation process. Aggregated predictions from all outer folds, covering 100% of the data points, were used to compute the explained variance (R^2) of foot placement predicted by the input modality. Under this nested cross-validation framework, it is possible, though unlikely, to obtain negative R^2 values, which occurs when the model fails to generalize to the testing dataset, performing worse than simply predicting the average foot placements (which would result in $R^2 = 0$). In such cases, the model's predictive power is minimal or nonexistent. To prevent overfitting, we used early stopping and dropout when training the neural networks, whereas L2 regularization is used to prevent overfitting to historical data or high-dimensional input space for linear models. Since neural networks are more complex than linear models, they inherently exhibit lower bias and higher variance. To mitigate this higher variance of neural networks and to better interpret model behavior across gait phases, we smooth the R^2 curves using local regression (LOWESS) and cubic spline.

To evaluate model performance, we assigned a score to each model based on the Root Mean Squared Error (RMSE). As the time window increases, the input contains accumulative information about the foot placement thereby enhancing the models' predictive power. We used the RMSE curve achieved by the swing-foot kinematics as a baseline, reflecting the predictive information inherently contained in the swing foot dynamics⁸⁰. We define the model score as the RMSE as defined in next section). The normalized model score is then computed relative to the model with the highest score. Formally, let $\text{RMSE}(m, \phi)$ denote the RMSE of model m at gait phase ϕ and let c denote the critical gait phase. We define the model score s_m :

$$s_m = \frac{1}{|\psi|} \sum_{\phi \in \psi} \frac{\min_{m'} \text{RMSE}(m', \phi)}{\text{RMSE}(m, \phi)}$$

where $\psi = \{0, 0.05, 0.10, \dots, c\}$, and the normalized model score s_m^n :

$$s_m^n = \frac{s_m}{\max_{m'} s_{m'}}$$

Note that the normalized model score is bounded within the interval $(0, 1]$, where the lower bound is approached when the RMSE is arbitrarily large, and the upper bound is achieved by the optimal model.

Quantifying the prediction timescale

The predictive power of foot placement using different input modalities across the gait cycle provides insight into the timescale of the control strategy. For an input modality to be considered a strong predictor, it must outperform the autoregressive baseline and demonstrate an earlier and larger increase in predictive power. To evaluate this, we identify the gait phase where the input modality achieves its maximum performance over the baseline, measured by the relative RMSE gap (Figure 5A). Beyond this phase, the input modality's contribution diminishes, as the predictive power of the swing foot itself increases at a faster rate.

To better understand swing foot prediction timescale, we aim to identify two critical timing events: (1) the time at which the swing foot begins its swing phase and (2) the time at which it starts containing significant information about future foot placement. The onset of swing phase is defined as the peak velocity of the swing foot along the fore-aft direction. From this peak, we trace backward to identify the point where the velocity drops below 5% of its maximal value (Figure 5B). This approach of anchoring the swing detection to the peak velocity ensures robustness and allows to avoid false positives.

Identification of relevant timepoints

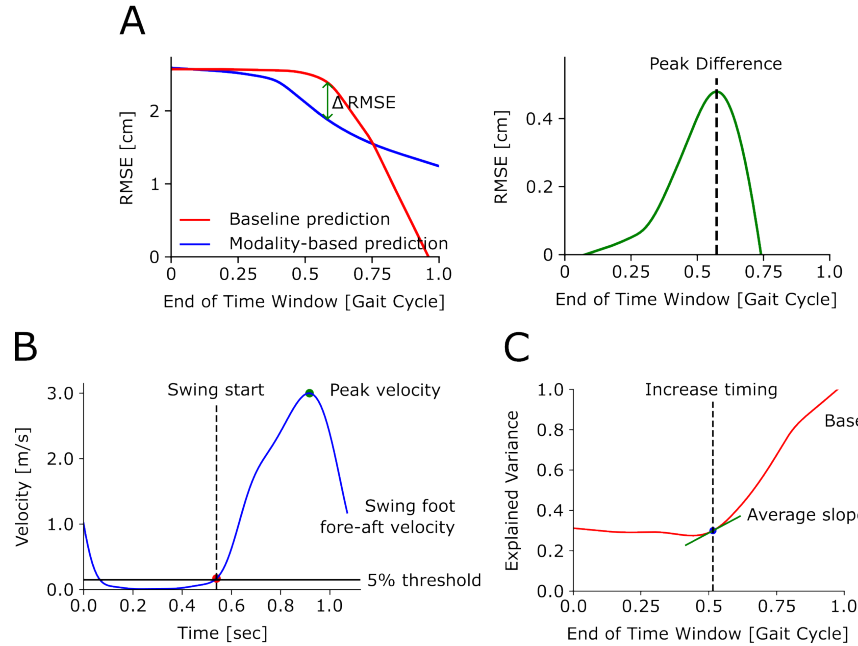


Figure 5. Identification of relevant timepoints. **A** The relative RMSE between modality-based predictions and the autoregressive baseline prediction as a function of gait phases. The timing of the peak difference indicates the phase where the input modality is the strongest predictor. **B** An example velocity curve along the locomotor axis, with the 5% of peak velocity threshold used to determine the onset of the swing phase. **C** The baseline R^2 curve, showing a breakpoint where R^2 increases significantly. The timing of this breakpoint is identified as the phase where the slope exceeds the average slope.

We analyze the autoregressive baseline R^2 curve to determine the time at which the swing foot kinematics begins predicting substantially the future foot placement. The R^2 curve typically shows a non-decreasing trend as the gait cycle progresses, eventually reaching $R^2 = 1$ at the final timestep. A notable “breakpoint” in the R^2 curve is the phase at which the predictive power of the swing foot kinematics sharply rises. To systematically identify this breakpoint, we calculate the average slope of the R^2 curve, defined as $r = R^2(1) - R^2(0)$, and locate the gait phase where the slope reaches its maximal value. We then trace backward from this gait phase to find the first point where the slope falls below the average slope, marking the critical transition phase (Figure 5C). This approach provides a robust method for identifying key transitions in the gait cycle and aligns with the underlying dynamics of gait and motor control.

Acknowledgments

Wei-Chen Wang was supported by a Mathworks EECS Fellowship and MIT Research Support Committee Grant. Antoine De Comite was supported by a K. Lisa Yang Ingergrative Computational Neuroscience (ICoN) Fellowship. This work is also supported by the McGovern Institute for Brain Research and the NSF Center for Integrative Movement Sciences Summer Institute. The authors declare no competing interests.

References

1. Peng, X. B., Abbeel, P., Levine, S. & Van de Panne, M. Deepmimic: Example-guided deep reinforcement learning of physics-based character skills. *ACM Transactions On Graph. (TOG)* **37**, 1–14 (2018).
2. Seethapathi, N. & Srinivasan, M. Step-to-step variations in human running reveal how humans run without falling. *Elife* **8**, e38371 (2019).
3. Balaji, E., Brindha, D., Elumalai, V. K. & Umesh, K. Data-driven gait analysis for diagnosis and severity rating of parkinson’s disease. *Med. Eng. & Phys.* **91**, 54–64 (2021).
4. Lanotte, F., O’Brien, M. K. & Jayaraman, A. Ai in rehabilitation medicine: opportunities and challenges. *Annals Rehabil. Medicine* **47**, 444–458 (2023).

5. Afschrift, M. *et al.* Assisting walking balance using a bio-inspired exoskeleton controller. *J. neuroengineering rehabilitation* **20**, 82 (2023).
6. Beck, O. N. *et al.* Exoskeletons need to react faster than physiological responses to improve standing balance. *Sci. robotics* **8**, eadf1080 (2023).
7. Wang, Y. & Srinivasan, M. Stepping in the direction of the fall: the next foot placement can be predicted from current upper body state in steady-state walking. *Biol. letters* **10**, 20140405 (2014).
8. Rankin, B. L., Buffo, S. K. & Dean, J. C. A neuromechanical strategy for mediolateral foot placement in walking humans. *J. neurophysiology* **112**, 374–383 (2014).
9. Bruijn, S. M. & Van Dieën, J. H. Control of human gait stability through foot placement. *J. The Royal Soc. Interface* **15**, 20170816 (2018).
10. De Comite, A. & Seethapathi, N. Foot placement control underlies stable locomotion across species. *bioRxiv* 2024–09 (2024).
11. Joshi, V. & Srinivasan, M. A controller for walking derived from how humans recover from perturbations. *J. The Royal Soc. Interface* **16**, 20190027 (2019).
12. Ingram, J. N. & Wolpert, D. M. Naturalistic approaches to sensorimotor control. *Prog. brain research* **191**, 3–29 (2011).
13. Matthis, J. S., Barton, S. L. & Fajen, B. R. The critical phase for visual control of human walking over complex terrain. *Proc. Natl. Acad. Sci.* **114**, E6720–E6729 (2017).
14. Lillicrap, T. P. *et al.* Continuous control with deep reinforcement learning. *arXiv preprint arXiv:1509.02971* (2015).
15. Radosavovic, I. *et al.* Humanoid locomotion as next token prediction. *Adv. Neural Inf. Process. Syst.* **37**, 79307–79324 (2025).
16. Lee, S.-W. & Asbeck, A. A deep learning-based approach for foot placement prediction. *IEEE Robotics Autom. Lett.* **8**, 4959–4966 (2023).
17. Xiong, J. *et al.* A probability fusion approach for foot placement prediction in complex terrains. *IEEE Transactions on Neural Syst. Rehabil. Eng.* **31**, 4591–4600 (2023).
18. Chen, X., Zhang, K., Liu, H., Leng, Y. & Fu, C. A probability distribution model-based approach for foot placement prediction in the early swing phase with a wearable imu sensor. *IEEE Transactions on Neural Syst. Rehabil. Eng.* **29**, 2595–2604 (2021).
19. Asogwa, C. O., Nagano, H., Wang, K. & Begg, R. Using deep learning to predict minimum foot–ground clearance event from toe-off kinematics. *Sensors* **22**, 6960 (2022).
20. Vetter, P. & Wolpert, D. M. Context estimation for sensorimotor control. *J. Neurophysiol.* **84**, 1026–1034 (2000).
21. Hayhoe, M. M. & Matthis, J. S. Control of gaze in natural environments: effects of rewards and costs, uncertainty and memory in target selection. *Interface focus* **8**, 20180009 (2018).
22. Patla, A. E. Understanding the roles of vision in the control of human locomotion. *Gait & posture* **5**, 54–69 (1997).
23. Warren, W. H. The dynamics of perception and action. *Psychol. review* **113**, 358 (2006).
24. Matthis, J. S. & Fajen, B. R. Visual control of foot placement when walking over complex terrain. *J. experimental psychology: human perception performance* **40**, 106 (2014).
25. Muller, K. S. *et al.* Foothold selection during locomotion in uneven terrain: Results from the integration of eye tracking, motion capture, and photogrammetry. *eLife* **12** (2024).
26. Shadmehr, R. & Krakauer, J. W. A computational neuroanatomy for motor control. *Exp. brain research* **185**, 359–381 (2008).
27. Seethapathi, N., Clark, B. C. & Srinivasan, M. Exploration-based learning of a stabilizing controller predicts locomotor adaptation. *Nat. Commun.* **15**, 9498 (2024).
28. Wolpert, D. M. & Ghahramani, Z. Computational principles of movement neuroscience. *Nat. neuroscience* **3**, 1212–1217 (2000).
29. Van Beers, R. J., Sittig, A. C. & Gon, J. J. D. v. d. Integration of proprioceptive and visual position-information: An experimentally supported model. *J. neurophysiology* **81**, 1355–1364 (1999).
30. Matthis, J. S., Yates, J. L. & Hayhoe, M. M. Gaze and the control of foot placement when walking in natural terrain. *Curr. Biol.* **28**, 1224–1233 (2018).

31. Sorensen, K., Hollands, M. A. & Patla, A. The effects of human ankle muscle vibration on posture and balance during adaptive locomotion. *Exp. brain research* **143**, 24–34 (2002).
32. Roden-Reynolds, D. C., Walker, M. H., Wasserman, C. R. & Dean, J. C. Hip proprioceptive feedback influences the control of mediolateral stability during human walking. *J. neurophysiology* **114**, 2220–2229 (2015).
33. Bent, L. R., Inglis, J. T. & McFadyen, B. J. When is vestibular information important during walking? *J. neurophysiology* **92**, 1269–1275 (2004).
34. van Dieën, J. H., Bruijn, S. M. & Afschrift, M. Assessment of stabilizing feedback control of walking: A tutorial. *J. Electromyogr. Kinesiol.* 102915 (2024).
35. Luo, S. *et al.* Robust walking control of a lower limb rehabilitation exoskeleton coupled with a musculoskeletal model via deep reinforcement learning. *J. neuroengineering rehabilitation* **20**, 34 (2023).
36. Sawicki, G. S., Beck, O. N., Kang, I. & Young, A. J. The exoskeleton expansion: improving walking and running economy. *J. neuroengineering rehabilitation* **17**, 1–9 (2020).
37. Voloshina, A. S. & Ferris, D. P. Biomechanics and energetics of running on uneven terrain. *The journal experimental biology* **218**, 711–719 (2015).
38. McGeer, T. Passive dynamic walking. *The international journal robotics research* **9**, 62–82 (1990).
39. Collins, S. H. *Dynamic walking principles applied to human gait*. Ph.D. thesis, University of Michigan (2008).
40. Blum, Y., Lipfert, S. W., Rummel, J. & Seyfarth, A. Swing leg control in human running. *Bioinspiration & biomimetics* **5**, 026006 (2010).
41. Cappellini, G., Ivanenko, Y. P., Poppele, R. E. & Lacquaniti, F. Motor patterns in human walking and running. *J. neurophysiology* **95**, 3426–3437 (2006).
42. Kuvulmaz, J., Usanmaz, S. & Engin, S. N. Time-series forecasting by means of linear and nonlinear models. In *MICAI 2005: Advances in Artificial Intelligence: 4th Mexican International Conference on Artificial Intelligence, Monterrey, Mexico, November 14–18, 2005. Proceedings 4*, 504–513 (Springer, 2005).
43. Hyndman, R. *Forecasting: principles and practice* (OTexts, Melbourne, Australia, 2018).
44. Nguyen, T. L., Gsponer, S., Ilie, I. & Ifrim, G. Interpretable time series classification using all-subsequence learning and symbolic representations in time and frequency domains. *arXiv preprint arXiv:1808.04022* (2018).
45. Cho, K. *et al.* Learning phrase representations using rnn encoder-decoder for statistical machine translation. *arXiv preprint arXiv:1406.1078* (2014).
46. Vaswani, A. *et al.* Attention is all you need. *Adv. neural information processing systems* **30** (2017).
47. Bai, S., Kolter, J. Z. & Koltun, V. An empirical evaluation of generic convolutional and recurrent networks for sequence modeling. *arXiv preprint arXiv:1803.01271* (2018).
48. Lea, C., Flynn, M. D., Vidal, R., Reiter, A. & Hager, G. D. Temporal convolutional networks for action segmentation and detection. In *proceedings of the IEEE Conference on Computer Vision and Pattern Recognition*, 156–165 (2017).
49. Franceschi, J.-Y., Dieuleveut, A. & Jaggi, M. Unsupervised scalable representation learning for multivariate time series. *Adv. neural information processing systems* **32** (2019).
50. Ismail Fawaz, H., Forestier, G., Weber, J., Idoumghar, L. & Muller, P.-A. Deep learning for time series classification: a review. *Data mining knowledge discovery* **33**, 917–963 (2019).
51. Bagnall, A., Lines, J., Bostrom, A., Large, J. & Keogh, E. The great time series classification bake off: a review and experimental evaluation of recent algorithmic advances. *Data mining knowledge discovery* **31**, 606–660 (2017).
52. Daley, M. A. & Biewener, A. A. Running over rough terrain reveals limb control for intrinsic stability. *Proc. Natl. Acad. Sci.* **103**, 15681–15686 (2006).
53. van der Linden, M. H., Marigold, D. S., Gabreëls, F. J. & Duysens, J. Muscle reflexes and synergies triggered by an unexpected support surface height during walking. *J. neurophysiology* **97**, 3639–3650 (2007).
54. Merel, J., Botvinick, M. & Wayne, G. Hierarchical motor control in mammals and machines. *Nat. communications* **10**, 5489 (2019).
55. Kuo, A. D. The relative roles of feedforward and feedback in the control of rhythmic movements. *Mot. control* **6**, 129–145 (2002).

56. Todorov, E. & Jordan, M. I. Optimal feedback control as a theory of motor coordination. *Nat. neuroscience* **5**, 1226–1235 (2002).
57. Maurus, P., Mahdi, G. & Cluff, T. Increased muscle coactivation is linked with fast feedback control when reaching in unpredictable visual environments. *iScience* **27** (2024).
58. Nayeem, R., Bazzi, S., Sadeghi, M., Hogan, N. & Sternad, D. Preparing to move: Setting initial conditions to simplify interactions with complex objects. *PLOS Comput. Biol.* **17**, e1009597 (2021).
59. Leestma, J. K., Golyski, P. R., Smith, C. R., Sawicki, G. S. & Young, A. J. Linking whole-body angular momentum and step placement during perturbed human walking. *J. Exp. Biol.* **226**, jeb244760 (2023).
60. van Dieën, J. H., Bruijn, S. M., Lemaire, K. K. & Kistemaker, D. A. Simultaneous stabilizing feedback control of linear and angular momentum in human walking. *bioRxiv* 2025–01 (2025).
61. MacLellan, M. J. & Patla, A. E. Adaptations of walking pattern on a compliant surface to regulate dynamic stability. *Exp. brain research* **173**, 521–530 (2006).
62. Hak, L., Houdijk, H., Beek, P. J. & van Dieën, J. H. Steps to take to enhance gait stability: the effect of stride frequency, stride length, and walking speed on local dynamic stability and margins of stability. *PloS one* **8**, e82842 (2013).
63. Schulz, B. W. Healthy younger and older adults control foot placement to avoid small obstacles during gait primarily by modulating step width. *J. neuroengineering rehabilitation* **9**, 1–10 (2012).
64. Collins, S. H. & Kuo, A. D. Two independent contributions to step variability during over-ground human walking. *PloS one* **8**, e73597 (2013).
65. Taheri, O., Ghorbani, N., Black, M. J. & Tzionas, D. Grab: A dataset of whole-body human grasping of objects. In *Computer Vision–ECCV 2020: 16th European Conference, Glasgow, UK, August 23–28, 2020, Proceedings, Part IV 16*, 581–600 (Springer, 2020).
66. Kratzer, P. *et al.* Mogaze: A dataset of full-body motions that includes workspace geometry and eye-gaze. *IEEE Robotics Autom. Lett.* **6**, 367–373 (2020).
67. Schwaner, M. *et al.* Future tail tales: A forward-looking, integrative perspective on tail research. *Integr. Comp. Biol.* **61**, 521–537 (2021).
68. Muramatsu, N., Shin, S., Deng, Q., Markham, A. & Patel, A. Wildpose: A long-range 3d wildlife motion capture system. *J. Exp. Biol.* jeb–249987 (2025).
69. Song, S. & Geyer, H. A neural circuitry that emphasizes spinal feedback generates diverse behaviours of human locomotion. *The J. physiology* **593**, 3493–3511 (2015).
70. Song, S. & Geyer, H. Evaluation of a neuromechanical walking control model using disturbance experiments. *Front. computational neuroscience* **11**, 15 (2017).
71. Caggiano, V., Wang, H., Durandau, G., Sartori, M. & Kumar, V. Myosuite—a contact-rich simulation suite for musculoskeletal motor control. *arXiv preprint arXiv:2205.13600* (2022).
72. Banks, J. J., Chang, W.-R., Xu, X. & Chang, C.-C. Using horizontal heel displacement to identify heel strike instants in normal gait. *Gait & Posture* **42**, 101–103 (2015).
73. Zeni Jr, J., Richards, J. & Higginson, J. Two simple methods for determining gait events during treadmill and overground walking using kinematic data. *Gait & posture* **27**, 710–714 (2008).
74. Hestness, J. *et al.* Deep learning scaling is predictable, empirically. *arXiv preprint arXiv:1712.00409* (2017).
75. Guo, C. & Berkhahn, F. Entity embeddings of categorical variables. *arXiv preprint arXiv:1604.06737* (2016).
76. Hochreiter, S. & Schmidhuber, J. Long short-term memory. *Neural computation* **9**, 1735–1780 (1997).
77. Karpathy, A. & Fei-Fei, L. Deep visual-semantic alignments for generating image descriptions. In *Proceedings of the IEEE conference on computer vision and pattern recognition*, 3128–3137 (2015).
78. Bates, S., Hastie, T. & Tibshirani, R. Cross-validation: what does it estimate and how well does it do it? *J. Am. Stat. Assoc.* **119**, 1434–1445 (2024).
79. Kingma, D. P. & Ba, J. Adam: A method for stochastic optimization. *arXiv preprint arXiv:1412.6980* (2014).
80. Takens, F. Detecting strange attractors in turbulence. In *Dynamical Systems and Turbulence, Warwick 1980: proceedings of a symposium held at the University of Warwick 1979/80*, 366–381 (Springer, 2006).

81. Yang, L. & Shami, A. On hyperparameter optimization of machine learning algorithms: Theory and practice. *Neurocomputing* **415**, 295–316 (2020).
82. Cawley, G. C. & Talbot, N. L. On over-fitting in model selection and subsequent selection bias in performance evaluation. *The J. Mach. Learn. Res.* **11**, 2079–2107 (2010).
83. Bergstra, J. & Bengio, Y. Random search for hyper-parameter optimization. *J. machine learning research* **13** (2012).

Supplementary Materials

Hyperparameter Tuning To ensure a fair comparison, we independently tune the hyperparameters for each model and input modality across all contexts using nested cross-validation^{81,82}. For hyperparameter optimization, we use grid search when the search space is manageable, and random search⁸³ when the hyperparameter space exceeds 100 configurations. Below, we outline the hyperparameter search space for each model. See the Methods section for details on model architecture.

- LSTM: the size of the LSTM hidden layer, $\text{hidden_dim} \in \{2, 4, 8, 16, 32, 64, 128, 256\}$.
- GRU: the size of the GRU hidden layer, $\text{hidden_dim} \in \{2, 4, 8, 16, 32, 64, 128, 256\}$.
- FCNN: the fully connected layers are designed such that the number of nodes in each layer decays exponentially, with a minimum of 8 nodes per layer and a guaranteed minimum number of layers. The decay factor, $\text{decay} \in \{2, 4, 8, 16\}$; the dropout rate, $\text{dropout} \in \{0, 0.1, 0.2, 0.3\}$.
- TCN: the size of the TCN block output size, $\text{hidden_dim} \in \{4, 8, 16\}$; the kernel size, $\text{kernel} \in \{1, 3, 5, 7\}$; dilation factor, $\text{dilation} \in \{1, 2, 4\}$; the dropout rate $\text{dropout} \in \{0, 0.1, 0.2, 0.3\}$.
- Transformer: the size of positional encoding, $\text{hidden_dim} \in \{16, 32, 64\}$; the number of layers, $\text{num_layers} \in \{2, 3, 4\}$; the number of attention heads, $\text{num_heads} \in \{2, 4, 8\}$; the size of feedforward dimension, $\text{ff_dim} \in \{16, 32, 64\}$; the dropout rate $\text{dropout} \in \{0, 0.1, 0.2, 0.3\}$.

After determining the optimal hyperparameters for each context, input modality, and model, we evaluate the predictive power with the identified hyperparameter configuration.

Predictive power across models The Methods section describes how the performances of the models are evaluated.

Predictive power across models (treadmill)

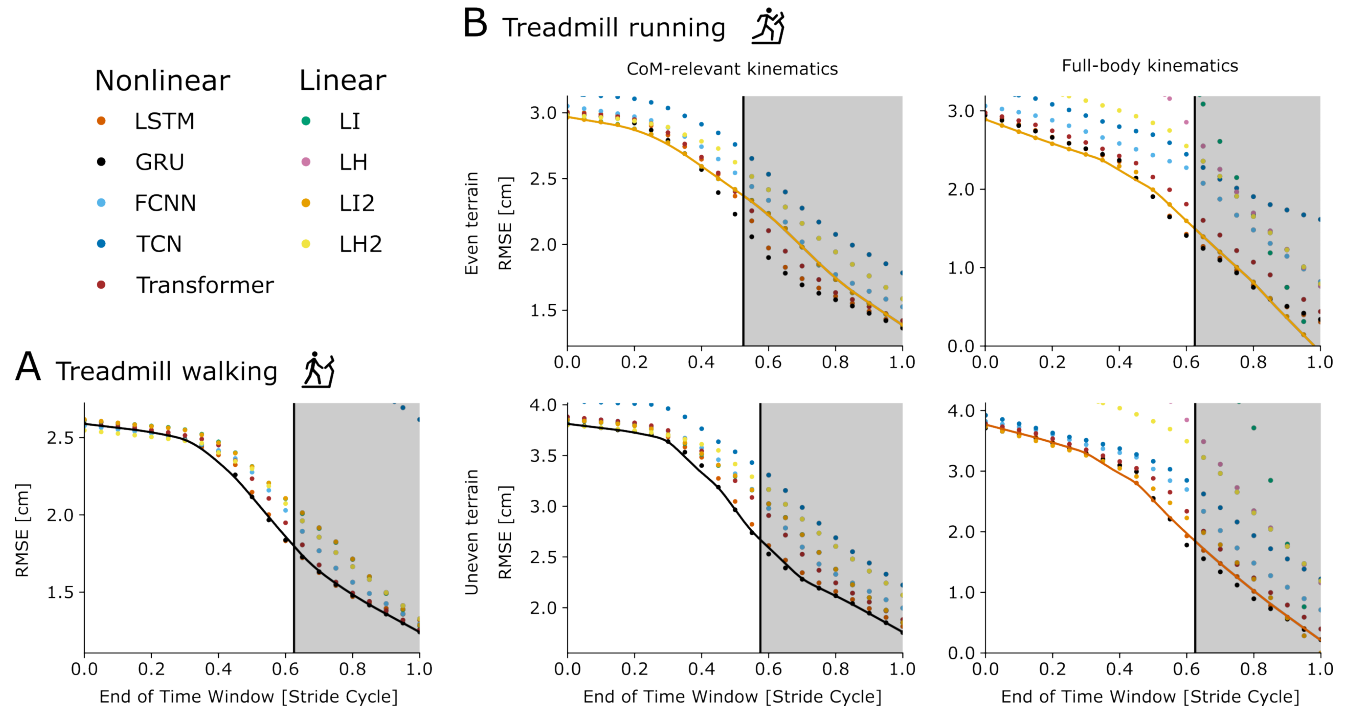



Figure 6. Predictive power across models. **A** Predictive power during treadmill walking. The vertical line indicates the critical phase when the relative predictive power is maximized, thereby only gait phases before the gray-shaded area are considered. The model with the average highest score prior to the critical phase was deemed optimal, and its predictive power is shown by the interpolated curve (LOWESS). See the Methods section for more details on the evaluation metric. The normalized model score is summarized in Table 1. **B** Predictive power during treadmill running.

Predictive power across models (overground)

Overground walking 

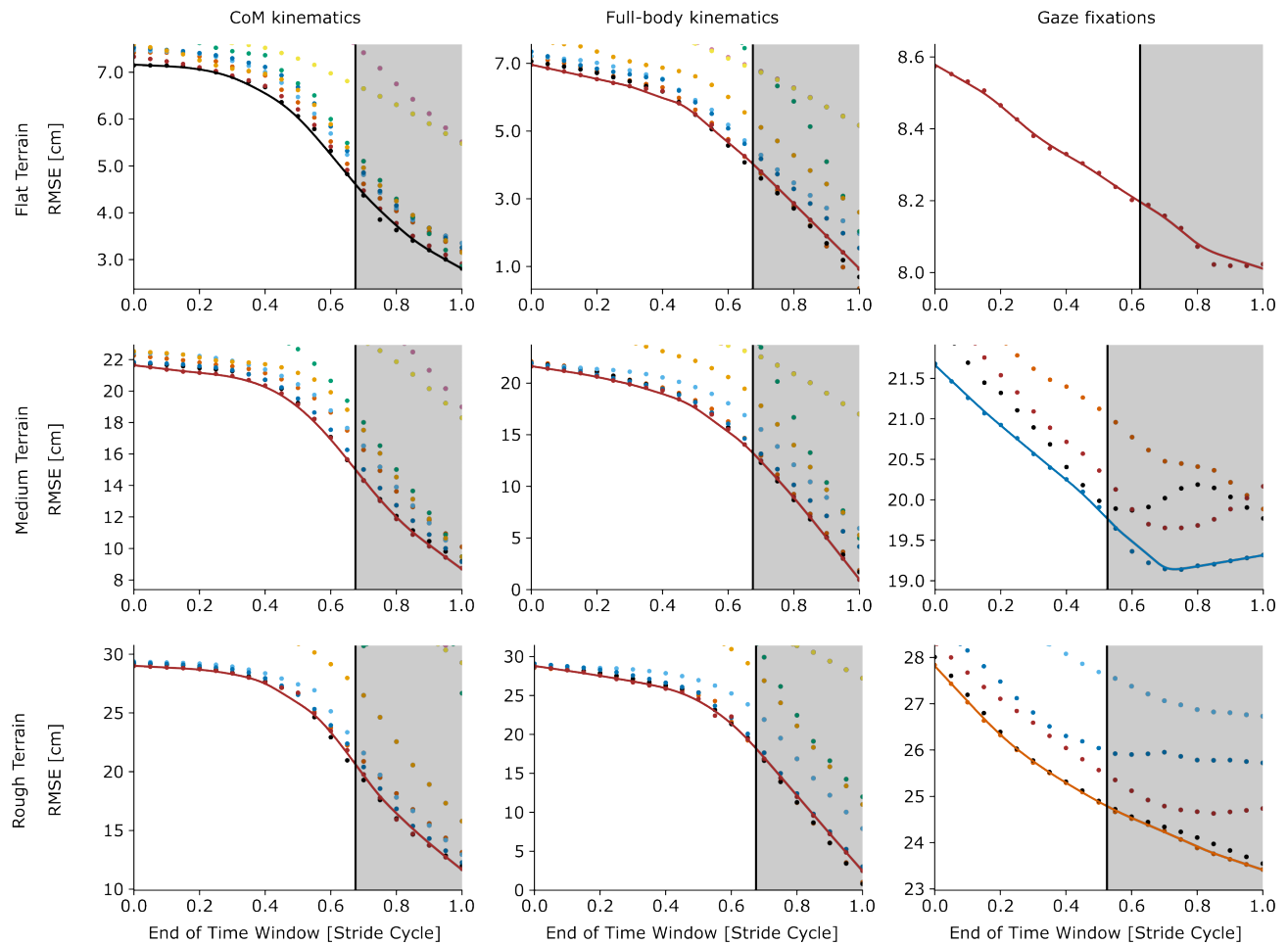


Figure 7. Predictive power across models during overground walking. See Figure 6 for details.

Relative predictive power across input modalities and contexts (fore-aft)

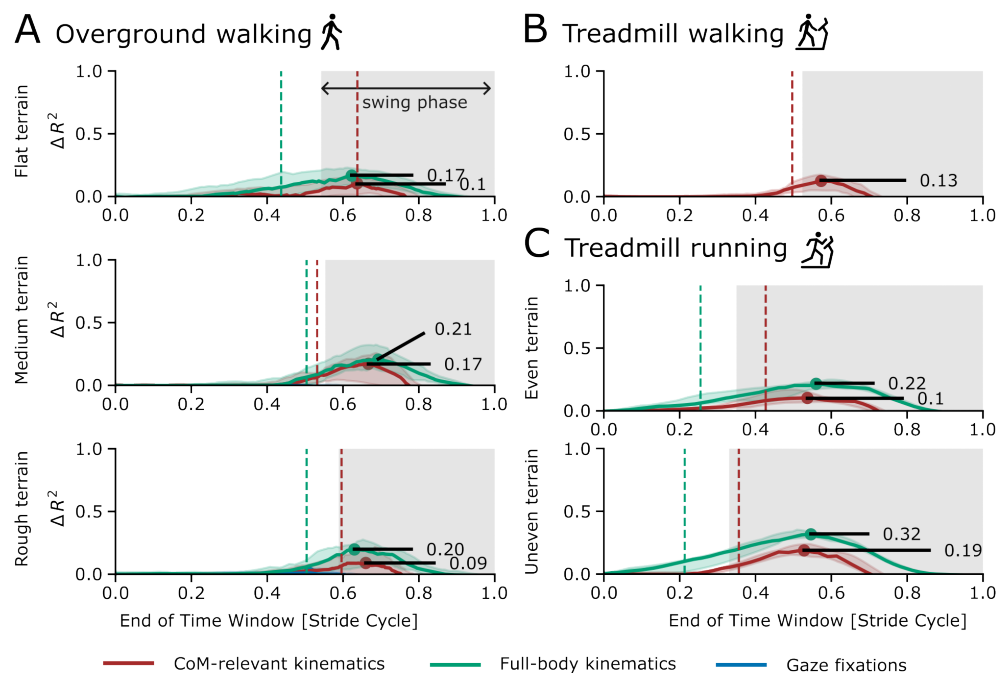


Figure 8. Relative predictive power across input modalities and contexts for fore-aft foot placement predictions during **A** Treadmill walking, **B** treadmill running, and **C** Overground walking. See Figure 2 for details.